BJR https://doi.org/10.1259/bjr.20220233

Received: 25 February 2022 | Accepted: 24 November 2022 | Published online: 23 January 2023

Cite this article as:
Adams DM, Boubertakh R, Miquel ME. Effects of spatial and temporal resolution on cardiovascular magnetic resonance feature tracking measurements using a simple realistic numerical phantom. *Br J Radiol* (2023) 10.1259/bjr.20220233.

FULL PAPER

Effects of spatial and temporal resolution on cardiovascular magnetic resonance feature tracking measurements using a simple realistic numerical phantom

[1]DAVID M ADAMS, MSc, [2]REDHA BOUBERTAKH, PhD and [1,3,4]MARC ERIC MIQUEL, PhD

[1]Clinical Physics, Barts Health NHS Trust, London, United Kingdom
[2]National Heart Research Institute Singapore (NHRIS), 5 Hospital Drive, Singapore
[3]Centre for Advanced Cardiovascular Imaging, NIHR Barts Biomedical Research Centre (BRC), William Research Institute, Queen Mary University of London, Charterhouse Square, London, United Kingdom
[4]Digital Environment Research Institute (DERI), Queen Mary University of London, London, United Kingdom

Address correspondence to:
Dr Marc Eric Miquel
E-mail: *m.e.miquel@qmul.ac.uk*
Mr David M Adams
E-mail: *david.adams@nhs.net*

Objectives To develop a single-slice numerical phantom with known myocardial motion, at several temporal and in-plane spatial resolutions, for testing and comparison of Cardiovascular Magnetic Resonance (CMR) feature tracking (FT) software.

Methods The phantom was developed based on CMR acquisitions of one volunteer (acquired cine, tagging cine, T1 map, T2 map, proton density weighted image). The numerical MRI simulator JEMRIS was used, and the phantom was generated at several in-plane spatial resolutions (1.4 × 1.4 mm^2 to 3.0 × 3.0 mm^2) and temporal resolutions (20 to 40 cardiac phases). Two feature tracking software packages were tested: Medical Image Tracking Toolbox (MITT) and two versions of cvi42 (v5.3.8 and v5.13.7). The effect of resolution on strain results was investigated with reference to ground-truth radial and circumferential strain.

Results Peak radial strain was consistently undermeasured more for cvi42 v5.13.7 than for v5.3.8. Increased pixel size produced a trend of increased difference from ground-truth peak strain, with the largest changes for cvi42 obtained using v5.13.7 between 1.4 × 1.4 mm^2 and 3.0 × 3.0 mm^2, at 9.17 percentage points (radial) and 8.42 percentage points (circumferential).

Conclusions The results corroborate the presence of intervendor differences in feature tracking results and show the magnitude of strain differences between software versions.

Advances in knowledge This study shows how temporal and in-plane spatial resolution can affect feature tracking with reference to the ground-truth strain of a numerical phantom. Results reaffirm the need for numerical phantom development for the validation and testing of FT software.

INTRODUCTION

Cardiovascular Magnetic Resonance (CMR) feature tracking (FT) uses optical flow methods to measure myocardial motion through the maximum likelihood frame-by-frame displacement of image features in regions of interest.[1] Optical flow can be combined with other techniques such as registration and edge detection to give an overall tracking method.[2] CMRFT was introduced in 2009[3] and has been applied to the analysis of the left ventricle (LV) more than the right,[4] although it is also used for atrial analysis.[1] CMRFT software is used to quantitatively analyse myocardial motion in standard clinical cine images by tracking contours through the cardiac cycle. It usually requires user input (endocardial and epicardial contours for one cardiac phase) and calculates indices such as strain that can reflect underlying myocardial contractile dysfunction.[1] Strain is a measure of the change in length of tissue in a given direction with respect to the length at end-diastole (ED).[2] Applications of CMRFT include assessment of ischemia, cardiomyopathies, congenital heart diseases, and quantification of dyssynchrony.[1,5]

FT has been compared to speckle tracking echocardiography (STE) and CMR tagging analysis, which likewise offer regional myocardial functional assessment.[6,7] STE, which is increasingly being used clinically, operates similarly to CMRFT, although tracking operates on speckle, present in ultrasound images.[8] CMR tagging analysis operates on images acquired using selectively induced perturbations of magnetization, forming a grid pattern in the myocardium, the deformation of which can be directly tracked making it the reference for strain quantification.[6] The main advantage of FT over CMR tagging is that FT uses the steady-state free precession (SSFP) cines that are routinely acquired in standard protocols to visually assess motion and to calculate left ventricular volumes, whereas CMR tagging requires additional sequences.[9] Furthermore, FT uses user-friendly, semi-automated software, with analysis based on myocardial contours, while CMR tagging analysis is more time-consuming.[9]

Limitations of FT include its relative inability to accurately measure regional myocardial strain.[6] Differences in measured myocardial strain between software packages, difficulties in establishing normal reference ranges for FT derived strain, and the lack of absolute validation, have hindered the clinical acceptance of FT.[6,10] Although the intervendor agreement, interobserver reproducibility, and intraobserver reproducibility of FT have been assessed,[3,11] showing significant differences in strain, these studies only investigated relative errors, without comparison to ground-truth. Absolute validation is needed in order to know the uncertainty of a given FT software package and will be useful in establishing the acceptable range of uncertainty. This requires cine images for which the ground-truth motion is known *a priori*, and consequently phantom images for which the deformation is fully controlled are ideal. This approach has already been successfully applied for the validation of two-dimensional STE software packages.[12] This study found relative errors of below 10%, which were considered acceptable by consensus of the European Association of Cardiovascular Imaging (EACVI) and the American Society of Echocardiography (ASE) standardization Task Force.[12] However, simulating CMR cine images is more complex than simulating echocardiographic images.

The ideal phantom for FT validation would exhibit controlled cardiac motion and morphology with full knowledge of ground-truth strain, as for an analytical numerical phantom, created using mathematical functions. It should also include the realistic anatomical features and image texture of a voxel-based phantom, created using clinical images. However, it is not possible to simultaneously realize controlled ground-truth and data realism using either approach.[13] The integration of these two phantom creation approaches produces a hybrid numerical phantom.[14]

One example of a hybrid numerical phantom for CMR is the Magnetic Resonance Extended Cardiac-Torso (MRXCAT) cine phantom, used to simulate novel image acquisition and reconstruction techniques.[14] However, it is not suitable for FT as it lacks simulation of realistic image structure, which is the basis of optical flow algorithms used by FT software. A different approach to hybrid phantom creation involved warping template cine sequences.[15] This approach was subsequently improved on[16] by using methods including MR physics simulation to avoid the texture warping caused by deforming template images.

The use of MR physics simulation permits the investigation of the effects of temporal and in-plane spatial resolution, as well as MR pulse sequence parameters, on FT performance. This facilitates the standardization of cine acquisitions for optimized FT performance. Reduced in-plane spatial resolution (increased voxel size) can impair FT by reducing the variation in pixel brightness due to tissue displacement. FT requires that in-plane spatial resolution is sufficient for the displacements of interest to be measured within the ability of the software to measure subpixel displacement.[17] Low temporal resolution can lead to transient spikes in motion being missed, potentially obscuring clinically significant motion.[2] It also causes interframe displacements to be large thus impairing FT, and image decorrelation (the reduction of the similarity of image features from frame to frame) that further impairs FT.[2] Conversely, high temporal resolution may not benefit, and may even impair, FT if not accompanied by increased in-plane spatial resolution, as frame-to-frame displacement is reduced relative to pixel size.[17]

The present work utilized a simple approach to hybrid numerical phantom generation for a single slice, with motion derived from image analysis, for the purpose of testing and comparing FT software. The study aimed to compare the strain results of two FT software packages, as well as two software versions of one of these software packages, to quantify the uncertainties associated with comparing FT results, as well as the effects of temporal and in-plane spatial resolution on FT performance, with reference to ground-truth strain.

METHODS AND MATERIALS

Phantom development

Short-axis images were acquired for one 33 y/o healthy adult male volunteer using a 1.5 T Siemens Magnetom Aera system (Siemens Healthineers, Erlangen, Germany) with a 30-element coil (combined thoracic and spine). Details of acquired sequences are given in Table 1.

The T1 map, T2 map, and proton density weighted image were registered to the left ventricle (LV) ED myocardial contours of the tagging cine (Figure 1) using control point registration. The control points were defined using a parametric mapping of the LV myocardium.[18] Points included the right ventricular insertion points, and the displacement field for registration was generated by diffusion of control point displacement vectors within and outside of the LV using iterative convolution with a Gaussian kernel.[19] Registered images were deformed from ED, generating a series of registered deformed images through the cardiac cycle. The myocardial deformation from ED was extracted from the tagging cine using the tagging analysis software CIMTag2D (version 8.1.5, Auckland MRI Research Group, New Zealand), and interpolated to cover the full field of view using a least squares fit. The displacement was applied over a dilated mask of the LV, and the displacement at the edge pixels of this region, and pixels directly adjacent to these, was averaged with displacement outside of the LV, extracted from B-spline-based non-rigid

Table 1. Cardiac Magnetic Resonance acquisition parameters

Sequence	bSSFP cine	SPAMM tagging cine	ED MOLLI T1 map	ED bSSFP T2 map	ED FLASH proton density weighted image
Field of view (mm×mm)	360 × 270	360 × 270	360 × 270	360 × 270	360 × 270
Acquisition matrix size	256 × 140	256 × 131	256 × 144	192 × 108	256 × 173
Reconstructed in-plane resolution (mm×mm)	1.41 × 1.41	1.41 × 1.41	1.41 × 1.41	1.41 × 1.41	1.41 × 1.41
Number of slices	12	1 (mid-LV)	1 (mid-LV)	1 (mid-LV)	1 (mid-LV)
Slice thickness (mm)	8	6	8	8	8
Number of cardiac phases	30	32	1 (ED)	1 (ED)	1 (ED)
Flip angle (°)	50	14	35	70	5
Echo spacing (ms)	2.79	4.63	3.90	3.33	10.50
Echo time (TE) (ms)	1.18	3.89	1.12	1.06	3.11
Number of segments	10	7	72	54	15
GRAPPA acceleration factor	2	1	2	2	1
Partial Fourier	Yes	Yes	Yes	Yes	No

ED, End-Diastole; FLASH, Fast Low Angle Shot; LV, Left Ventricle;MOLLI, Modified Look-Locker Imaging; SPAMM, Spatial Modulation of Magnetization; bSSFP, Balanced Steady-State Free Precession.

registration[20] through the acquired balanced Steady-State Free Precession (bSSFP) cine (Figure 1), to smoothly merge these deformations. A zero-end-displacement condition was applied to reduce unrealistic deformation at the end of the cardiac cycle. The series of registered deformed images was inputted to the numerical MRI simulator JEMRIS[21] to simulate a bSSFP sequence, giving the cine frames of the numerical phantom.

The numerical phantom (DICOM series) was generated with a range of temporal and in-plane spatial resolutions. The in-plane spatial resolution was altered by adjusting the *k*-space matrix size of the simulation in JEMRIS, and the temporal resolution by temporally interpolating the displacement applied to the ED images inputted to JEMRIS, using cubic b-spline interpolation. The in-plane spatial resolution values were 1.4 × 1.4, 2.0 × 2.0, 2.5 × 2.5, and 3.0 × 3.0 mm^2, for 30 cardiac phases. The temporal resolution values (ms) were 61.65, 49.32, 41.10, 35.23, and 30.83, corresponding to 20, 25, 30, 35, and 40 cardiac phases, respectively, all with 1.4 × 1.4 mm^2 in-plane spatial resolution.

Feature tracking analysis

The resulting numerical phantom was analysed with two FT software packages: Medical Image Tracking Toolbox (MITT),[22] and cvi42 (Circle Cardiovascular Imaging Inc., Calgary, Canada). For cvi42, two versions were used: v5.3.8 and the latest available version, v5.13.7. The analysis was carried out using endocardial and epicardial LV contours defined at ED. The strain results were compared with the ground-truth 2D Lagrangian strain values. In addition to strain, ground-truth displacement was calculated and compared to the FT results. For further details, see the Appendix provided as supplementary material.

RESULTS

The phantom, developed based on acquired images, correctly represented the ground truth motion, showed realistic image texture, and had contrast typical of clinical bSSFP cine images (Figure 2), at varying temporal and in-plane spatial resolution.

Figure 3 shows a comparison of the global strain results of the two FT software packages with the analytical ground-truth strain curves.

Figures 4 and 5, respectively, show the strain results for the range of in-plane spatial resolutions and temporal resolutions of the numerical phantom. Peak strain magnitude was undermeasured with reference to ground-truth strain in all cases, except for radial strain for pixel sizes 2.5 × 2.5 mm^2 and 3.0 × 3.0 mm^2 using MITT. For cvi42, peak radial strain was consistently undermeasured more for v5.13.7 than for v5.3.8. At the default temporal and in-plane spatial resolution (30 cardiac phases and 1.4 × 1.4 mm^2), the differences between the two versions of cvi42 were 0.69 percentage points (radial) and 0.07 percentage points (circumferential). The largest differences in peak strain between the two versions were 2.40 percentage points for radial strain, measured for 30 cardiac phases at 2.5 × 2.5 mm^2 pixel size, and 1.01 percentage points for circumferential strain, measured for 30 cardiac phases at 3.0 × 3.0 mm^2 pixel size.

Figure 6 shows how in-plane spatial resolution and temporal resolution affected the magnitude of relative difference from ground-truth peak strain. Increased pixel size produced a trend of increased difference between measured peak strain and ground-truth peak strain. This effect was most prominent for radial strain

Figure 1. The method for numerical phantom creation. The acquired end-diastole images (a) were used to generate the registered end-diastole images (d) by registration to the myocardial contours of the tagging cine (b) at end-diastole. The myocardial displacement fields (c)(x-direction and y-direction) were obtained from the tagging cine using tagging analysis, and full displacement fields (f) were obtained from the short-axis balanced steady-state free precession (bSSFP) cine (e) using B-spline-based non-rigid registration. (c) and (f) were merged to give (g). (g), and (g) interpolated to different temporal resolutions, were applied to (d) to give 5 sets of proton density (PD) weighted, T2, and T1 cines (h). These were inputted (phase-by-phase) to JEMRIS (Jülich Extensible MRI Simulator), producing four simulated cines with 30 cardiac phases and differing spatial resolutions (i), and four simulated cines with 1.4 × 1.4 mm^2 and differing temporal resolutions (j).

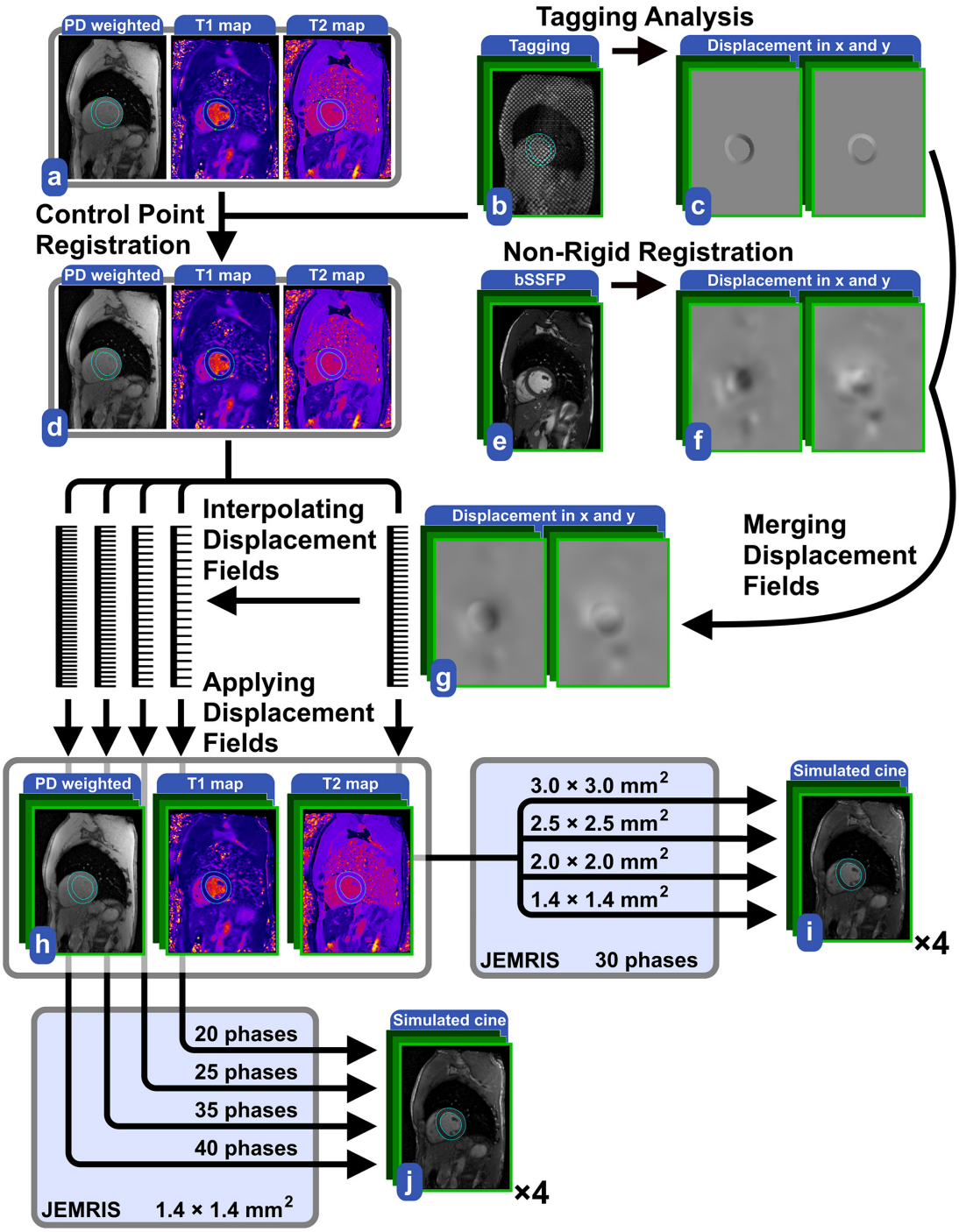

Figure 2. Selected frames of the simulated single-slice short-axis balanced steady-state free precession (bSSFP) cine at the default temporal and in-plane spatial resolution (30 cardiac phases and 1.4 × 1.4 mm^2).

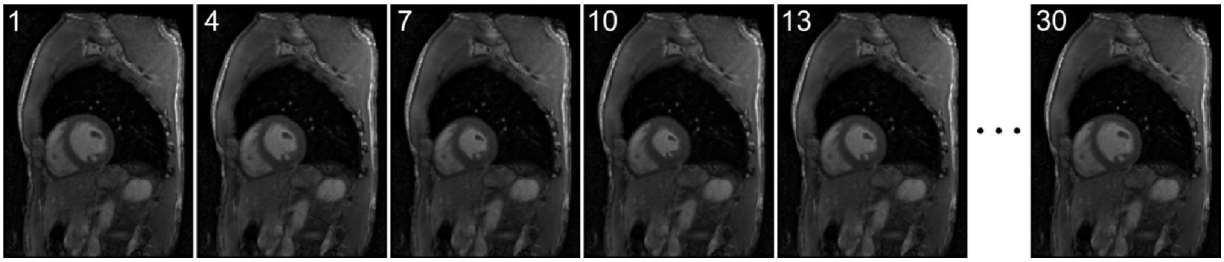

with MITT, with large differences for 2.5 × 2.5 mm^2 and 3.0 × 3.0 mm^2 pixel size. For MITT, the largest increases in magnitude of relative difference between measured peak strain and ground-truth peak strain with pixel size were 203.44 percentage points between pixel sizes of 2.0 × 2.0 mm and 3.0 × 3.0 mm^2 for radial strain, and 4.47 percentage points between pixel sizes of 1.4 × 1.4 mm and 3.0 × 3.0 mm^2 for circumferential strain. For cvi42, these were obtained using v5.13.7 between pixel sizes of 1.4 × 1.4 mm^2 and 3.0 × 3.0 mm^2, at 9.17 percentage points for radial strain and 8.42 percentage points for circumferential strain. Comparing the two versions of cvi42, absolute differences between measured peak strain and ground-truth peak strain increased with pixel size more for v5.13.7 than for v5.3.8. Figure 6 shows that no clear trend in relative difference between measured peak strain and ground-truth peak strain was observed for temporal resolution. For temporal resolution, the largest changes in the magnitude of relative difference between measured peak strain and ground-truth peak strain were obtained between 20 and 25 cardiac phases, at 1.43 percentage points for radial strain using cvi42 v5.3.8, and 1.67 percentage points for circumferential strain using cvi42 v5.13.7.

Figure 3. Comparison of the ground-truth global (a) radial strain and (b) circumferential strain with results from MITT and the two versions of cvi42 tested.

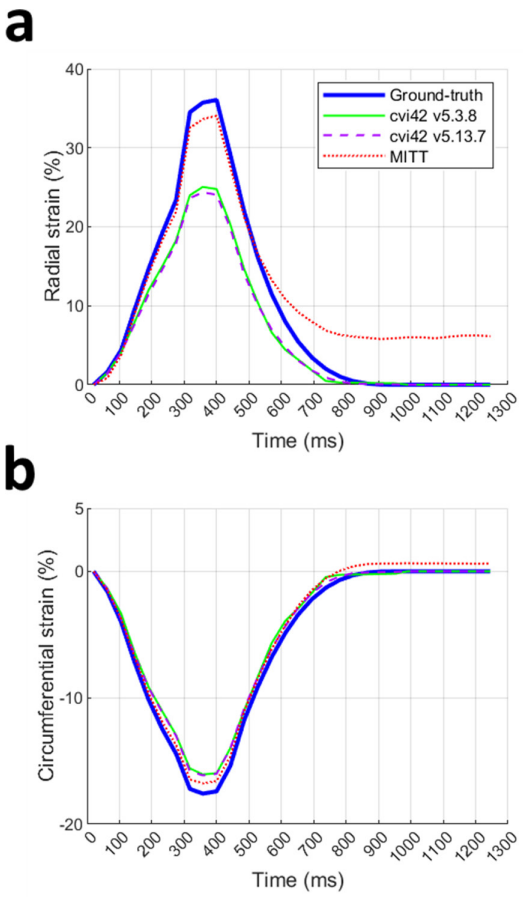

Figures 7 and 8, respectively, show the displacement results for the range of in-plane spatial resolutions and temporal resolutions of the numerical phantom.

A video showing FT and ground-truth motion for the series with 30 cardiac phases and a range of in-plane spatial resolutions is provided as supplementary material.

DISCUSSION

The observation that peak radial strain was consistently undermeasured more for v5.13.7 than for v5.3.8 appears to correspond with cvi42 v5.13.7 consistently measuring less radial displacement than cvi42 v5.3.8 (with the exception of the series with 20 cardiac phases). However, global radial and circumferential displacement do not reveal the full tracking data, and 2D radial strain is dependent on shear, which was not reported by cvi42. Analysis of strain results for volunteer data (see the Appendix provided as supplementary material) add support to the degree of differences in strain results between cvi42 software versions, with cvi42 v5.12.1 measuring lesser strain values than cvi42 v5.3.8. Peak radial and circumferential strain were most closely measured by MITT, although large differences from ground-truth peak radial strain were observed for pixel sizes 2.5 × 2.5 mm^2 and 3.0 × 3.0 mm^2, caused by large differences from ground-truth circumferential displacement. These large differences could possibly be reduced by deviating from the default FT parameters in MITT.

The trend identified in this study, increased difference between measured peak strain and ground-truth peak strain with increased pixel size, is congruent with the expectation of a reduction in FT accuracy as the limit of the ability of the software to measure subpixel displacement is approached. The result of no clear trend in relative difference between measured peak strain and ground-truth peak strain with temporal resolution suggests

Figure 4. Comparison of ground-truth global strain with feature tracking results at a range of in-plane spatial resolutions for (a) radial strain from v.5.3.8, (b) radial strain from v5.13.7, (c) radial strain from MITT, (d) circumferential strain from v5.3.8, (e) circumferential strain from v5.13.7, and (f) circumferential strain from MITT.

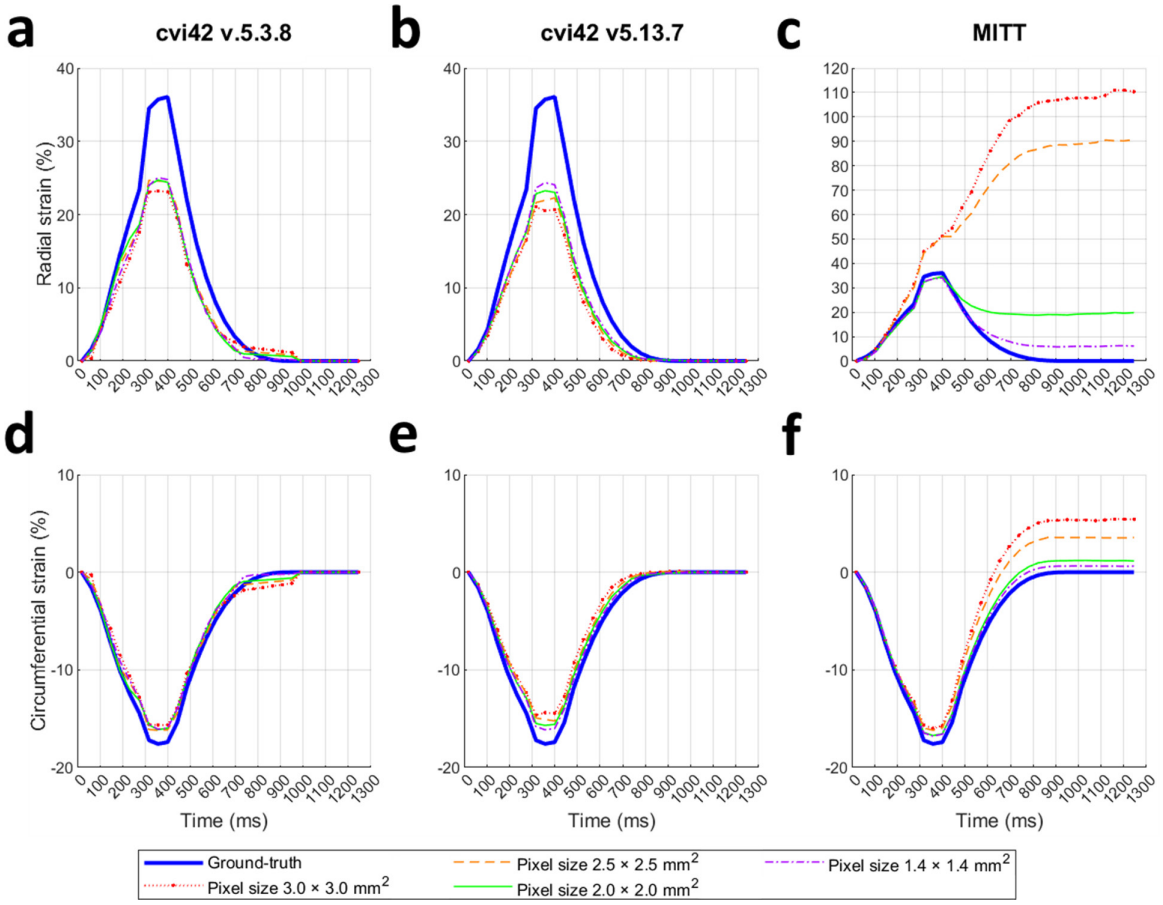

a minimal effect of temporal resolution on FT performance in this study.

Circumferential displacement for cvi42 v5.3.8 showed extensive variation through the cardiac cycle. This variation appeared to be rigid rotation of the tracked points, not affecting strain results.

Considering tracking post-systole, ground-truth strain was more closely followed by cvi42 v5.13.7 than cvi42 v5.3.8, particularly as pixel size was increased. MITT did not perform well post-systole, with large residual strain and displacement measured at the end of the cardiac cycle.

Intervendor and intravendor (between software versions) differences between measured strain and ground-truth strain could be attributable to differences in FT algorithms, as well as differences in post-tracking regularization. As for STE software, FT software may utilise proprietary methods of regularization including temporal and spatial smoothing, and models of normal cardiac deformation.[23] As information about FT algorithms and regularization is not generally available to users of FT software, it would be beneficial to implement testing of software after software updates, ideally via absolute validation using suitable numerical phantoms.

The minimum pixel size used for the numerical phantom was equal to that of the bSSFP cine used clinically ($1.4 \times 1.4\,mm^2$), and this was increased to a maximum of $3.0 \times 3.0\,mm^2$. This range, and the range of number of cardiac phases (20–40 cardiac phases), were chosen to broadly cover the ranges used with FT (1–2 mm in-plane spatial resolution, 25–35 cardiac phases).[6] The range used is similar to the overall range used in recent studies assessing the variation in FT results for acquisitions at different resolutions ($1.3 \times 1.3\,mm^2$ to $3.0 \times 3.0\,mm^2$ pixel size, 20–50 cardiac phases).[24–26]

The maximum differences between peak strain measurements and ground-truth strain obtained in the present study (excluding the large differences at pixel sizes of $2.5 \times 2.5\,mm^2$ and $3.0 \times 3.0\,mm^2$ for MITT) can be considered alongside the maximum differences in peak strain found in recent studies that investigated the effect of resolution on FT for non-phantom images. In a study by Backhaus et al,[24] for $n = 12$ healthy volunteers and $n = 9$ heart failure patients, maximum absolute differences of between 1.7 and 2.5% were found between 20 and 50 cardiac phases for circumferential strain. By comparing FT results for cines of differing temporal resolution directly, the differences found by Backhaus et al[24] reflect the effects of temporal resolution on FT performance as well as the effect of undersampling cardiac

Figure 5. Comparison of ground-truth global strain with feature tracking results at a range of temporal resolutions for (a) radial strain from v.5.3.8, (b) radial strain from v5.13.7, (c) radial strain from MITT, (d) circumferential strain from v5.3.8, (e) circumferential strain from v5.13.7, and (f) circumferential strain from MITT.

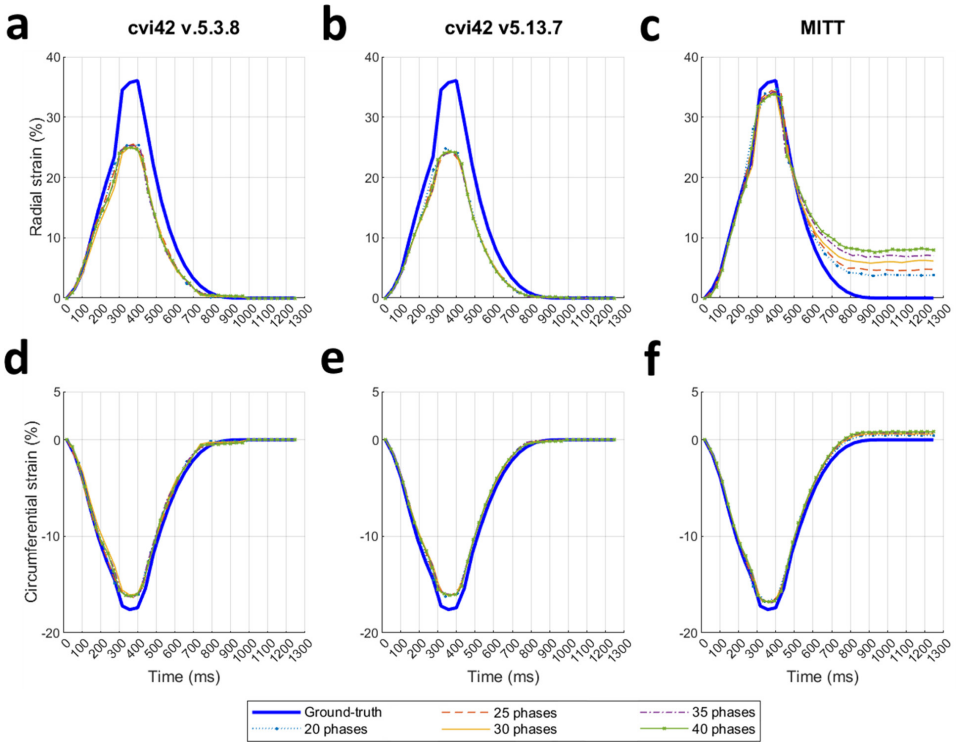

Figure 6. Magnitude of relative difference from ground-truth peak strain when varying (a, b, c) the in-plane spatial resolution and (d, e, f) the temporal resolution of the numerical phantom, for cvi42 v5.3.8 (a and d), cvi42 v5.13.7 (b and e), and MITT (c and f).

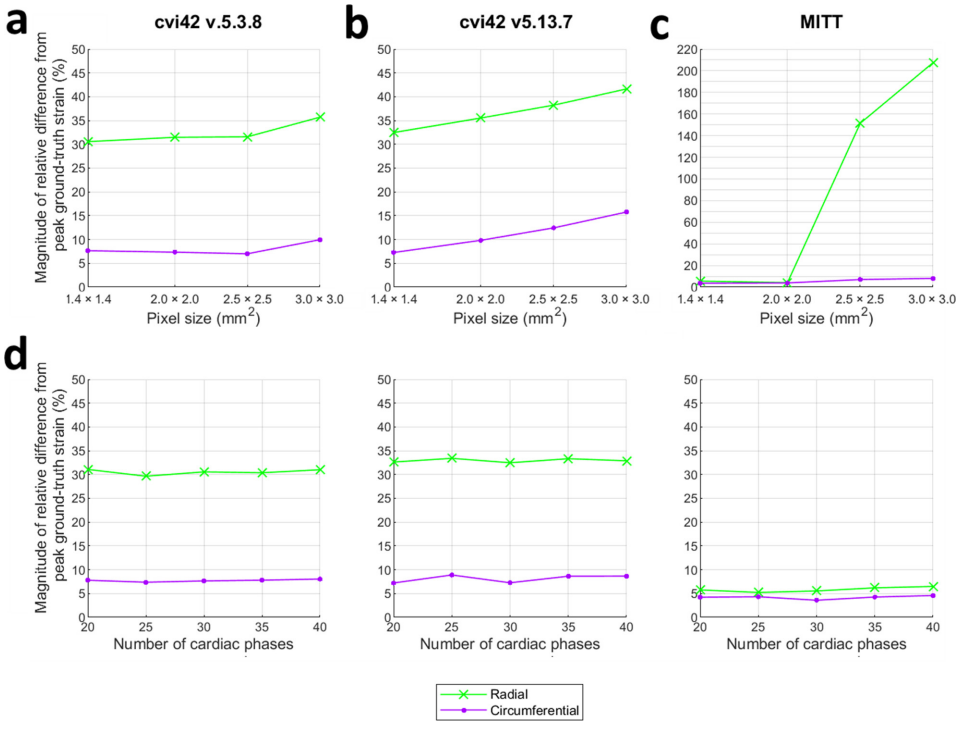

Figure 7. Comparison of ground-truth displacement with feature tracking results at a range of in-plane spatial resolutions for (a) radial displacement from v.5.3.8, (b) radial displacement from v5.13.7, (c) radial displacement from MITT, (d) circumferential displacement from v5.3.8, (e) circumferential displacement from v5.13.7, and (f) circumferential displacement from MITT.

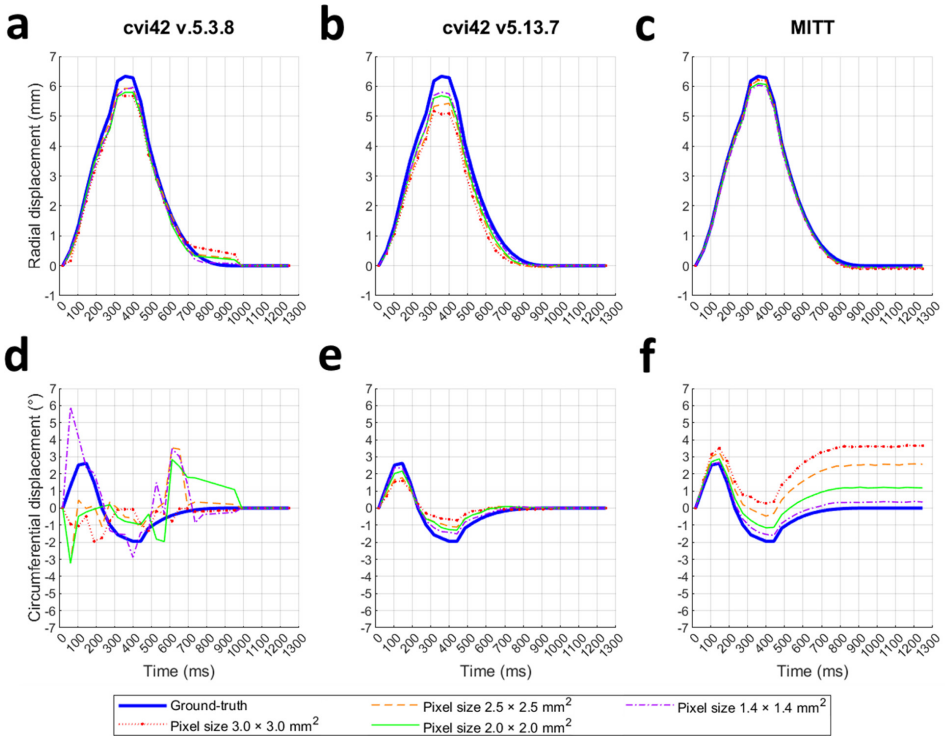

Figure 8. Comparison of ground-truth displacement with feature tracking results at a range of temporal resolutions for (a) radial displacement from v.5.3.8, (b) radial displacement from v5.13.7, (c) radial displacement from MITT, (d) circumferential displacement from v5.3.8, (e) circumferential displacement from v5.13.7, and (f) circumferential displacement from MITT.

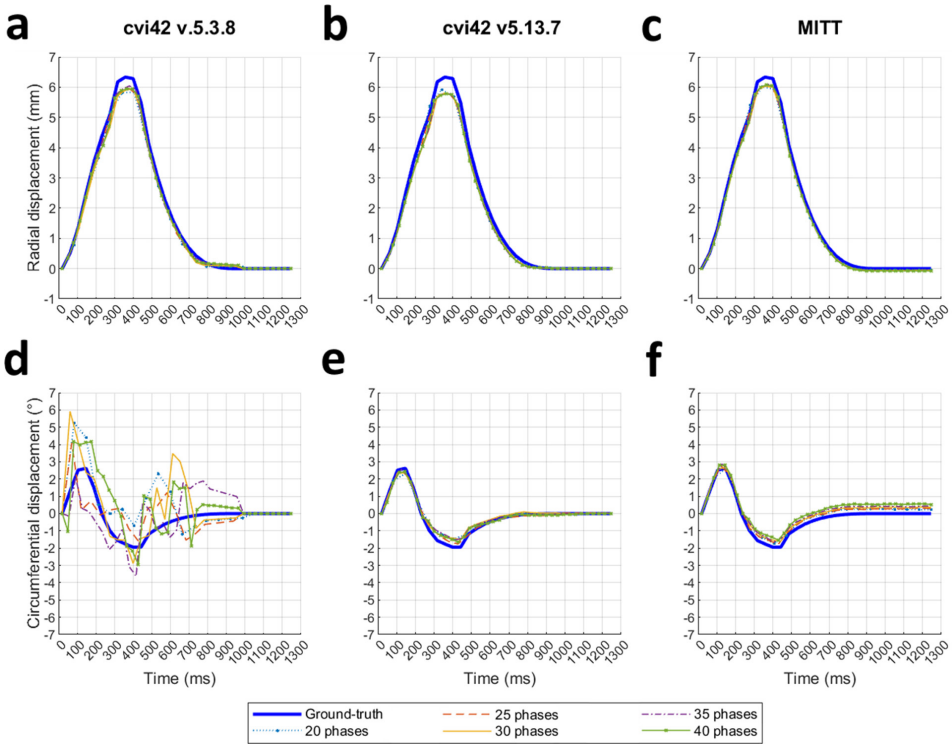

motion when temporal resolution is low. The results for temporal resolution demonstrated in the present study have excluded the effect of undersampling cardiac motion, which is an advantage of numerical phantom studies (see the Appendix provided as supplementary material for more information). In a study by von Knobelsdorff-Brenkenhoff et al,[25] for $n = 25$ with chronic myocardial infarct, significant differences were found when comparing $2.0 \times 2.0\,mm^2$ and $1.4 \times 1.4\,mm^2$ spatial resolutions: $36.8 \pm 19.0\%$ vs. $31.0 \pm 16.3\%$, $p = 0.013$ for radial strain, and $-18.6 \pm 5.6\%$ vs. $-14.6 \pm 10.9\%$, $p = 0.002$ for circumferential strain. However, spatial resolution was not found to significantly affect radial and circumferential strains for $n = 50$ healthy volunteers in the same study,[25] nor for $n = 12$ healthy volunteers and $n = 9$ heart failure patients in Backhaus et al's study[24] (in-plane spatial resolution from $1.5 \times 1.5\,mm^2$ to $3.0 \times 3.0\,mm^2$). It is noted that 2D Lagrangian strain is used with cvi42 in the present study and with cmr42 in von Knobelsdorff-Brenkenhoff et al's study,[25] whereas 1D Lagrangian strain was used with QStrain (Medis Medical Imaging Systems, Leiden, Netherlands) by Backhaus et al.[24] The strain definition affects strain values[27] and therefore affects the range of variability with resolution.

Limitations

While work towards producing numerical phantoms with sufficient realism to enable validation of FT software is ongoing, work by Zhou et al[16] in particular shows promising results towards this aim. The numerical phantom produced in the present work lacks such realism. In particular, the phantom does not include through-plane motion, myocardial intensity changes through the cardiac cycle, and temporal variation of the blood-pool. Therefore, the results presented here can only be used to make preliminary conclusions about the accuracy of FT software. Although the numerical phantom was limited to only one short-axis slice, this does not majorly compromise the validity of its use in testing FT software, besides results being limited to two-dimensional FT at the mid-LV. This is because, as verified by observation of cvi42 FT data, results for a given slice are not affected by the number of short-axis slices used in FT. Furthermore, many studies have carried out FT using only a single mid-LV slice, as highlighted in a recent review.[28] The inclusion of a long-axis slice, to test three-dimensional FT and longitudinal strain, would extend the utility of the phantom. Additionally, the method of numerical phantom generation limited the cardiac motion to that present in acquired images, whereas electromechanical models of the heart have been used in other studies to generate variable cardiac motion.[15,16] Finally, FT software of only two vendors was evaluated. Future studies should work towards absolute validation of all available FT software to allow intervendor comparisons.

CONCLUSION

This work presents a method to generate simple realistic numerical phantoms for the purpose of testing FT software. The results corroborate the presence of intervendor differences in FT results, and show the magnitude of the strain differences between software versions. This study shows how temporal and in-plane spatial resolution can affect FT with reference to the ground-truth strain of a numerical phantom. Results reaffirm the need for numerical phantom development for the validation and testing of FT software.

ACKNOWLEDGEMENTS

Dr Kenneth Fung, Matthieu Ruthven

REFERENCES

1. Schuster A, Hor KN, Kowallick JT, Beerbaum P, Kutty S. Cardiovascular magnetic resonance myocardial feature tracking: concepts and clinical applications. *Circ Cardiovasc Imaging* 2016; **9**(4): e004077. https://doi.org/10.1161/CIRCIMAGING.115.004077
2. Pedrizzetti G, Claus P, Kilner PJ, Nagel E. Principles of cardiovascular magnetic resonance feature tracking and echocardiographic speckle tracking for informed clinical use. *J Cardiovasc Magn Reson* 2016; **18**(1): 51. https://doi.org/10.1186/s12968-016-0269-7
3. Schuster A, Stahnke V-C, Unterberg-Buchwald C, Kowallick JT, Lamata P, Steinmetz M, et al. Cardiovascular magnetic resonance feature-tracking assessment of myocardial mechanics: intervendor agreement and considerations regarding reproducibility. *Clin Radiol* 2015; **70**: 989–98. https://doi.org/10.1016/j.crad.2015.05.006
4. Qu YY, Li H, Rottbauer W, Ma GS, Buckert D, Rasche V. Right ventricular free wall longitudinal strain and strain rate quantification with cardiovascular magnetic resonance based tissue tracking. *Int J Cardiovasc Imaging* 2020; **36**: 1985–96. https://doi.org/10.1007/s10554-020-01895-5
5. Muser D, Castro SA, Santangeli P, Nucifora G. Clinical applications of feature-tracking cardiac magnetic resonance imaging. *World J Cardiol* 2018; **10**: 210–21. https://doi.org/10.4330/wjc.v10.i11.210
6. Amzulescu MS, de Craene M, Langet H, Pasquet A, Vancraeynest D, Pouleur AC, et al. Myocardial strain imaging: review of general principles, validation, and sources of discrepancies. *Eur Heart J Cardiovasc Imaging* 2019; **20**: 605–19. https://doi.org/10.1093/ehjci/jez041
7. van Everdingen WM WM, Zweerink A, Nijveldt R, Salden OAE, Meine M, Maass AH, et al. Comparison of strain imaging techniques in CRT candidates: CMR tagging, CMR feature tracking and speckle tracking echocardiography. *Int J Card Imaging* 2018; **34**: 443–56.
8. Collier P, Phelan D, Klein A. A test in context: Myocardial strain measured by speckle-tracking echocardiography. J Am Coll Cardiol 2017;69:1043-1056.
9. Dardeer AM, Hudsmith L, Wesolowski R, Clift P, Steeds RP. The potential role of feature tracking in adult congenital heart disease: advantages and disadvantages in measuring myocardial deformation by cardiovascular magnetic resonance J Congenit Cardiol 2018;2.
10. Harries I, Liang K, Williams M, Berlot B, Biglino G, Lancellotti P, et al. Magnetic resonance imaging to detect cardiovascular effects of cancer therapy: JACC cardiooncology state-of-the-art review. J Am Coll Cardiol 2020;2:270–92.

11. Barreiro-Pérez M, Curione D, Symons R, Claus P, Voigt JU, Bogaert J. Left ventricular global myocardial strain assessment comparing the reproducibility of four commercially available CMR-feature tracking algorithms. *Eur Radiol* 2018; **28**: 5137–47. https://doi.org/10.1007/s00330-018-5538-4
12. D'hooge J, Barbosa D, Gao H, Claus P, Prater D, Hamilton J, et al. Two-Dimensional speckle tracking echocardiography: standardization efforts based on synthetic ultrasound data. *Eur Heart J Cardiovasc Imaging* 2016; **17**: 693–701. https://doi.org/10.1093/ehjci/jev197
13. Tobon-Gomez C, De Craene M, McLeod K, Tautz L, Shi W, Hennemuth A, et al. Benchmarking framework for myocardial tracking and deformation algorithms: an open access database. *Med Image Anal* 2013; **17**: 632–48. https://doi.org/10.1016/j.media.2013.03.008
14. Wissmann L, Santelli C, Segars WP, Kozerke S. MRXCAT: realistic numerical phantoms for cardiovascular magnetic resonance. *J Cardiovasc Magn Reson* 2014; **16**: 63. https://doi.org/10.1186/s12968-014-0063-3
15. Duchateau N, Sermesant M, Delingette H, Ayache N. Model-Based generation of large databases of cardiac images: synthesis of pathological cine Mr sequences from real healthy cases. *IEEE Trans Med Imaging* 2018; **37**: 755–66. https://doi.org/10.1109/TMI.2017.2714343
16. Zhou Y, Giffard-Roisin S, de Craene M, Camarasu-Pop S, D'Hooge J, Alessandrini M, et al. A framework for the generation of realistic synthetic cardiac ultrasound and magnetic resonance imaging sequences from the same virtual patients. *IEEE Trans Med Imaging* 2018; **37**: 741–54. https://doi.org/10.1109/TMI.2017.2708159
17. Hor KN, Baumann R, Pedrizzetti G, Tonti G, Gottliebson WM, Taylor M, et al. Magnetic resonance derived myocardial strain assessment using feature tracking. J Vis Exp 2011;48:2356.
18. Garcia-Barnes J, Gil D, Badiella L, Hernàndez-Sabaté A, Carreras F, Pujades S, et al. A normalized framework for the design of feature spaces assessing the left ventricular function. IEEE Trans Med Imaging 2010;29:733–45.
19. Prakosa A, Sermesant M, Delingette H, Marchesseau S, Saloux E, Allain P, et al. Generation of synthetic but visually realistic time series of cardiac images combining a biophysical model and clinical images. IEEE Trans Med Imaging 2013;32:99–109.
20. B-spline Grid. Image and Point based Registration - File Exchange - MATLAB Central. Kroon D-J. [updated 2011 March 16; cited 2022 February 7]. Available from: https://uk.mathworks.com/matlabcentral/fileexchange/20057-b-spline-grid-image-and-point-based-registration
21. Stöcker T, Vahedipour K, Pflugfelder D, Shah NJ. High-Performance computing MRI simulations. *Magn Reson Med* 2010; **64**: 186–93. https://doi.org/10.1002/mrm.22406
22. Queiros S, Morais P, Barbosa D, Fonseca JC, Vilaca JL, D'Hooge J. MITT: medical image tracking toolbox. *IEEE Trans Med Imaging* 2018; **37**: 2547–57. https://doi.org/10.1109/TMI.2018.2840820
23. Voigt J-U, Pedrizzetti G, Lysyansky P, Marwick TH, Houle H, Baumann R, et al. Definitions for a common standard for 2D speckle tracking echocardiography: consensus document of the EACVI/ASE/industry Task force to standardize deformation imaging. *Eur Heart J Cardiovasc Imaging* 2015; **16**: 1–11. https://doi.org/10.1093/ehjci/jeu184
24. Backhaus SJ, Metschies G, Billing M, Schmidt-Rimpler J, Kowallick JT, Gertz RJ, et al. Defining the optimal temporal and spatial resolution for cardiovascular magnetic resonance imaging feature tracking. *J Cardiovasc Magn Reson* 2021; **23**(1): 60. https://doi.org/10.1186/s12968-021-00740-5
25. von Knobelsdorff-Brenkenhoff F, Schunke T, Reiter S, Scheck R, Höfling B, Pilz G. Influence of contrast agent and spatial resolution on myocardial strain results using feature tracking MRI. *Eur Radiol* 2020; **30**: 6099–6108. https://doi.org/10.1007/s00330-020-06971-x
26. Bourfiss M, Steensma BR, te Riele A, Leiner T, Velthuis BK, Raaijmakers AJE. Feature-tracking cardiac magnetic resonance of the right ventricle: effect of field strength, resolution and imaging sequence. *Eur J Radiol* 2021; **138**: 109671. https://doi.org/10.1016/j.ejrad.2021.109671
27. Wehner GJ, Jing L, Haggerty CM, Suever JD, Chen J, Hamlet SM, et al. Comparison of left ventricular strains and torsion derived from feature tracking and DENSE CMR. *J Cardiovasc Magn Reson* 2018; **20**.
28. Vo HQ, Marwick TH, Negishi K. MRI-derived myocardial strain measures in normal subjects. *JACC Cardiovasc Imaging* 2018; **11**: 196–205.